Suppression of ELMs by Resonant Magnetic Perturbations in DIII-D in the ITER Similar Shape

J.S. deGrassie[1], M.J. Lanctot[1], D.M. Orlov[2], P.B. Snyder[1], T.E. Evans[1], M.E. Fenstermacher[3], G.L. Jackson[1], R. Nazikian[4], and M.R. Wade[1]

[1]*General Atomics, P.O. Box 85608, San Diego, California 92186-5608, USA*
[2]*University of California-San Diego, La Jolla, California, 92093, USA*
[3]*Lawrence Livermore National Laboratory, Livermore, CA 94550, USA*
[4]*Princeton Plasma Physics Laboratory, Princeton, NJ 08543, USA*

1. Introduction

In DIII-D it has been found that externally imposed small resonant magnetic perturbations (RMPs) can achieve complete ELM suppression with good confinement [1,2]. In these ELM-suppressed conditions in DIII-D the edge pedestal pressure profile is relaxed and falls into the region of stability for peeling-ballooning modes, as determined by the ELITE code [3], in that the result of the added RMP is to lower the edge pressure profile gradient away from the instability threshold for ELMs. It is not yet clear the detailed role of "resonant" in the spectrum of the applied perturbations, and how this relates to the limited regions in q_{95} in which RMP ELM suppression occurs in DIII-D, with q_{95} being the safety factor evaluated at $\tilde{\psi} = 0.95$, in normalized poloidal flux. Here, we describe the addition of RMP fields in DIII-D using a single row of the I-coils [4] in the configuration that applies an n=3 perturbation field, where n is the toroidal mode number of the perturbation.

RMP ELM suppression has been achieved in DIII-D at the ITER-design value of $I/aB = 1.415$ [5] in the ITER-design shape cross section, scaled down by a factor of 3.7, referred to as the ITER Similar Shape (ISS). The discharge conditions are at the ITER baseline scenario relevant values of β_N=1.7, H_{98}=1.1, and $\nu^*_{e\_ped} = 0.05$, with $I/aB = 1.39$. These parameters have their standard meanings [5], with $\nu^*_{e\_ped}$ being the electron collisionality at the top of the pedestal. The q_{95} window for ELM suppression in DIII-D is more readily extended to lower values with a single row in comparison with the typical double row standard suppression window. Presumably this is related to the difference in the mode content of applied field for one versus two rows.

To date the q_{95} windows for ELM suppression DIII-D have invariably been defined using the so-called JT-parameterized EFIT equilibria reconstructions [6], serving to sort the experimental results well [2]. However, these q_{95} values may not be accurate in detail to locate rational surfaces in the H-mode pedestal region because the localized edge bootstrap current is not included, nor measured. In Sec. 4 we discuss this further. Using standard JT EFITs, the q_{95} for this ISS suppression is 3.18 whereas the most robust ELM suppression window with two I-coil rows in DIII-D is at q_{95}~3.5 [1,2,4].

2. ELM Suppression

ELM Suppression in an ISS discharge is shown in the time traces in Fig. 1. After the RMP is turned on, I_{RMP} Fig. 1(a), the ELMs die away and eventually conditions settle into complete ELM suppression for $t > 6500$ ms, as seen in the D_α trace. The intervening clumps of ELMs are likely due to having a marginal level of the RMP field for suppression, an issue when energizing only one of the two rows of the I-coils. Other traces shown in Fig. 1 are β_N, (b), which is controlled here by feedback of the neutral beam injection (NBI) power in DIII-D, q_{95}, (b), H_{98}, (b), and $\nu^*_{e\_ped}$, (c), the pedestal electron collisionality.

Other factors within these ISS discharges in DIII-D may have contributed to ELM triggering in otherwise stable conditions. With RMPs applied these discharges had core MHD mode activity, which may have been playing a role in triggering the ELMs in the RMP period shown in Fig. 1. Another potential mechanism is that when using feedback controlled NBI to hold β_N at a fixed value, the instantaneous beam power can vary significantly in a short period of time since the individual neutral beam sources are limited to being either "on" or "off". The plasma energy integrates such switched-mode amplifier feedback, but the portion of the toroidal mass acceleration driven by the prompt torque [7] responds on the switching time scale. The resulting change of the velocity in the pedestal region may be large enough to affect the plasma screening of the externally applied RMPs [8] and affect ELM stability.

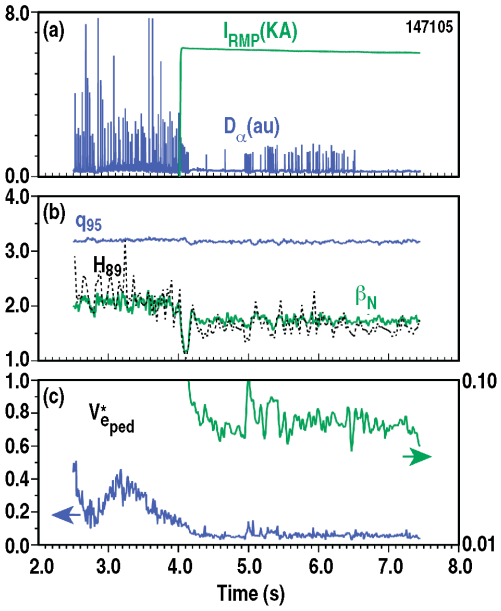

Fig. 1. RMP-induced ELM suppression in an ITER-similar discharge in DIII-D using a single I-coil row. (a) RMP amplitude (kA) and D_α (au), (b) q_{95}, H_{89} confinement parameter and β_N, (c) pedestal collisionality parameter, $\nu^*_{e\_ped}$, linear (lhs) and log (rhs) scale.

3. Pedestal Stability

In RMP ELM suppressed regimes in DIII-D it has been found that the ELITE MHD stability code [3] predicts that the pedestal should be stable to peeling-ballooning modes, hypothesized to be the trigger for ELMs [3], whereas in ELMing conditions in the same experiments ELITE predicts instability [9]. This is also the case with RMP ELM suppression in the ISS conditions described here.

The stability results of ELITE calculations for the discharge in Fig. 1 are shown in Fig. 2, with Fig. 2(a) showing the result before the RMP pulse is applied, t = 3750 ms, and Fig. 2(b) with the RMP pulse as the first period of ELM suppressed conditions is realized, t = 4250 ms. These plots show stability contours as scaled growth rates vs a normalized pedestal pressure gradient and a normalized pedestal current density [9]. The cross-hair symbols show where the measured pedestal conditions fall on the stability diagrams.

The ELITE stability analysis potentially provides a sufficient condition for RMP ELM suppression that would allow comparison between devices and projection to future machines. The details of the dynamics of how the RMP fields hold the pedestal below the instability threshold are the topic of ongoing research, both experimentally and theoretically.

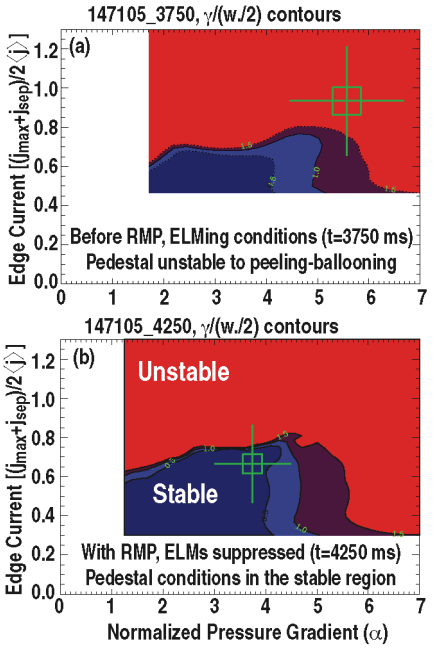

Fig. 2. ELITE stability boundaries and operating points (a) before and (b) after RMP ELM suppression in Fig. 1. Above the boundary line is the region of instability.

4. RMP Spectra

If there is an important spectral difference between the single I-coil row and the double row in DIII-D with ISS conditions it is not readily seen in two of the standard analysis tools used to examine the RMP field amplitude within the plasma. First, Fig. 3 shows mode

amplitude contours for the vacuum applied RMP field as computed by the SURFMN code [10]. The n=3 modal amplitude contours are shown for the actual condition used in the experiment in Fig. 3(a), upper row only with I_{RMP} = 6 kA, while in Fig. 3(b) we show a hypothetical case for the same plasma equilibrium with both rows having I_{RMP} = 3 kA, in the standard phasing where upper and lower I-coils at the same toroidal angle have the same sign of current. This comparison is done with constant total Ampere turns. In Fig. 3 the horizontal axis is the poloidal mode number, m, the vertical axis is $\tilde{\psi}$, and the amplitude scales are the same for Fig. 3(a,b). The left-handed twist is resonant, m<0. The dashed line traces out the resonant path along $q(\tilde{\psi}) = -m/3$ for the unperturbed axisymmetric EFIT-computed equilibrium.

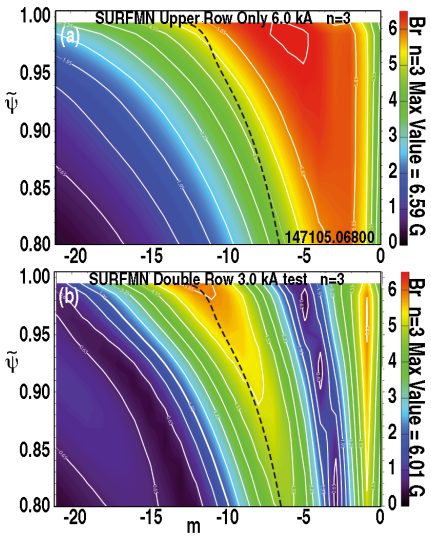

Fig. 3. SURFMN calculations of contours of the surface-averaged vacuum radial magnetic perturbation fields, b_{m3}, (a) for the single row I-coil used in Fig. 1 and (b) a double row model condition with 1/2 the single row current. The black dashed line shows the resonant q profile.

Comparing the amplitudes of the resonant surface-normal mode perturbation magnetic field amplitudes, b_{m3}, we see that the equivalent double row has slightly larger resonant values along the q path in the pedestal region than with the single row in the experiment. For example, in Fig. 3, the double (single) row value at the edge of the computation, $\tilde{\psi} \approx 0.995$, is 6.0 (5.4) Gauss, and at $\tilde{\psi} \approx 0.90$ it is 5.2 (4.8) Gauss. Yet experiments on DIII-D have indicated better ELM suppression results with the single row in this ISS scenario regime than with the double row operating at significantly larger I-coil current than 3 kA. One obvious feature in Fig. 3(a) is the large region of higher amplitude non-resonant b_{m3} inside the q path, that is, where $|m|<3q$. This is due to the "monopole" nature of the single row, giving a broad decaying spectrum in $|m|$, while the double row shows the interference pattern of a "dipole" launcher, having the resonant peak at nonzero m. The non-resonant fields may be playing an important role in the ELM suppression process, whereas it is usually the resonant components and the issues of plasma screening that are thought to be important [8]. The fact that only certain q values show the ELM suppression in DIII-D indicates something is q resonant, at least at the I-coil currents attainable.

The response of the plasma to the vacuum RMP fields changes the actual b_{m3} in the plasma [8]. We use MARS-F to compute the field perturbation spectral amplitude including this response effect [11] and again find there is no clear significant difference in the comparison between the double and single rows, other than the monopole versus dipole difference seen with SURFMN. Near the plasma edge the response has a kink-like feature that is also similar for single versus double row.

5. Suppression and q_{95}

In quoting the q_{95} values for the suppression windows in DIII-D the equilibria from JT EFITs are typically used. However for the ELITE stability and the MARS-F plasma response calculations, as well as the SURFMN plots, kinetic EFITs (KEFITs) have been used, which include also the internal magnetic field measurements and the measured kinetic pressure profiles for the electrons and ions in the fitting algorithm, allowing an edge bootstrap current [6]. With a fixed total plasma current, I_p, the added bootstrap current in the pedestal tends to raise the q values inside relative to a JT EFIT since there is less current inside and more added outside.

The change in the value of q_{95} between the two equilibrium computation methods is

relatively small, but it can be large enough to matter in the tight confines of the pedestal region where it is important to determine the location of a m/n=3 resonant layer relative to the pressure pedestal. The q profiles for these two methods before and after RMP ELM suppression are shown in Fig. 4(a), for the discharge from Fig. 1. Here, a q profile is plotted as m=3q versus $\tilde{\psi}$, in the edge region. The curves with solid circles are from KEFITs before the RMP is turned on, pre-RMP is shown by the upper curve (black online), and the other during RMP ELM suppression (red online). The downward shift is due to the computed change in the edge bootstrap current due to the RMP. In going from the JT EFIT to the KEFIT at the same time we see that the m value increases by approximately unity, thereby changing which m harmonic layer might be near the middle of the pedestal. The KEFITs show a near unity drop in m, at $\tilde{\psi} = 0.95$, with RMP suppression conditions relative to pre-RMP. All these EFITs come to a common q value near $\tilde{\psi} = 0.98$, perhaps a better sorting value when modifications to the bootstrap current can take place.

In Fig. 4(b) we look at the edge electron pressure profile vs q, again represented by m=3q. The q profile is monotonically increasing and can be used unambiguously as the radial coordinate. The upper curve is pre-RMP (black) and the lower with suppression (red). The dashed curve is the pre-RMP profile scaled uniformly down to the lower curve to be equal at q=2. The similarity in the electron pressure profiles inside the m=8/3 surface is clear, with the lower, ELM suppressed, P_e profile shape eroded in the region covered by the 9/3 and 10/3 surfaces. One theory postulates a resonant surface at the top of the RMP-reduced pedestal which limits further pedestal growth, thereby avoiding instability [5]. Another possibly meaningful aspect of Fig. 4(b) is the location of the 11/3 surface at the bottom of the pressure pedestal. If more than one resonant surface must be appropriately positioned to avoid ELMs, then the q_{95} windows for suppression would be more sparse than if only resonance at the pedestal top is needed.

Our point is to show the importance of accurate measurements of edge current profile in understanding the juxtaposition of the pressure pedestal and the resonant surfaces in the H-mode pedestal. While great care has been taken in constructing these KEFITs there are still limitations in accurately locating the resonant surfaces to within a small fraction of their separation.

This work was supported by the U.S. Department of Energy under DE-FC02-04ER54698, DE-FG02-95ER54309, DE-AC52-07NA27344, DE-FG02-05ER54809, and DE-AC02-09CH11466.

[1] T.E. Evans et al, Phys. Plasmas **13**, 056121 (2006)
[2] O. Schmitz et al, Nucl. Fusion **52**, 043005 (2012)
[3] P.B. Snyder et al, Phys. Plasmas **9**, 2037 (2002)
[4] M.E. Fenstermacher et al, Nucl. Fusion **48**, 122001 (2008)
[5] E.J. Doyle et al, Nucl. Fusion **50**, 075005 (2010)
[6] L.L. Lao et al, Fusion Sci, & Technol. **48**, 968 (2005)
[7] J.S. deGrassie et al, Phys. Plasmas **13**, 112507 (2006)
[8] N.M. Ferraro et al, Phys. Plasmas **19**, 056105 (2012)
[9] P.B. Snyder et al, Nucl. Fusion **47**, 961 (2007)
[10] M.J. Schaffer et al, Nucl. Fusion **48**, 024004 (2008)
[11] M.J. Lanctot et al, "Complete Suppression of Large Type-I Edge Localized Modes Using Multi-Harmonic Magnetic Perturbations in DIII-D," submitted Nucl. Fusion (2013).

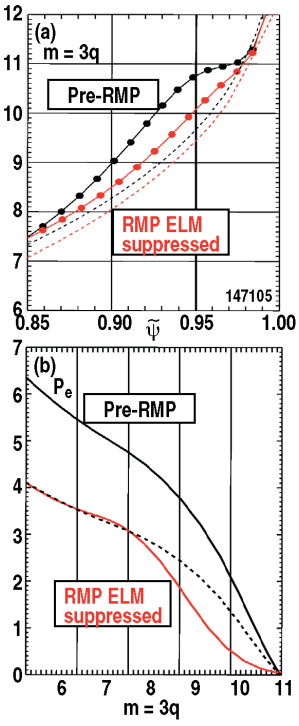

Fig. 4. (a) Edge m=3q profiles using Kinetic efits (solid circles) and JT efits (dashed lines) before (upper) and after (lower) RMP ELM suppression. (b) Edge electron pressure profile vs q before (upper) and after (lower) RMP ELM suppression. The dashed curve is the upper scaled to the lower at q=2.